SEISMIC RESPONSE DISTRIBUTION EXPRESSIONS FOR ROCKING BUILDING CONTENTS UNDER ORDINARY GROUND MOTIONS

A. K. Kazantzi,[1*] **C. G. Lachanas**[2] and **D. Vamvatsikos**[2]

[1]*Resilience Guard GmbH, Steinhausen, Switzerland.*

[2]*School of Civil Engineering, National Technical University of Athens, Athens, Greece.*

Keywords: earthquake engineering, rocking, building contents, floor motions, seismic fragility.

Abstract. *Analytical expressions are proposed for predicting the rocking response of rigid free-standing building contents subjected to seismic-induced floor excitations. The study considers a wide range of rigid block geometries and seismic floor acceleration histories that were recorded during actual earthquakes in instrumented Californian buildings, so as to cover, in a fully probabilistic manner, the entire spectrum of potential pure rocking responses, i.e. from the initiation of rocking up to the block overturning. Contrary to past observations on anchored building contents (prior to any failure in their anchorage system that could alter their response and mode of failure), it is shown that the response of free-standing blocks is not influenced by the predominant period of the supporting structure. The proposed set of equations can be utilised for estimating the response statistics and consequently for undertaking an analytical seismic fragility assessment on rocking building contents.*

1 INTRODUCTION

Non-structural components represent a significant part in a building's investment value and its operability. Hence, any seismic-induced damages to these elements are anticipated to have a substantial footprint in consequent financial integrity, business continuity, and resilience. The risk of non-structural damages is even higher if one considers that they could be triggered at lower, and yet more frequent, seismic intensity levels than those required to induce damages in structural elements, at least in modern buildings where stringent quality assurance standards have been exercised during construction. Apparently, non-structural damages are not only likely to occur more frequently than structural ones, but could also render an otherwise intact critical facility, e.g., a hospital or an airport, unusable for a substantial amount of time. Furthermore, apart from their impact on economy and business continuity aspects, building contents often represent invaluable cultural heritage items, such as museum artefacts (e.g. Parisi and Augenti, 2013; Spyrakos *et al*, 2016), in which case the associated losses are considered unacceptable from a social, cultural and historical standpoint.

Depending on their sensitivity to different damage metrics, non-structural components are classified by FEMA 356 (FEMA, 2000) into two major categories; the deformation-sensitive and the acceleration-sensitive ones. The damage in deformation-sensitive components is primarily induced by the drifts or deformations of the supporting structure. By contrast, the damage in acceleration-sensitive components is due to the imposed inertia forces that are developed during ground shaking. With reference to acceleration-sensitive components, these could be further discretised into those that are fully anchored to the supporting structure, those that are unanchored, and those that are partially anchored, as their anchorage is not designed to

[*] Corresponding author: nancy.kazantzi@resilienceguard.ch

withstand earthquake loading. In the latter two cases, assuming that a non-earthquake designed anchorage will more likely fail under seismic excitation, the (essentially free-standing) components, could undergo sliding, rocking, a combined response mode that includes both rocking and sliding, or overturning when subjected to base (ground or floor) accelerations.

Up until now, several studies have investigated the seismic response of free-standing building contents. Nevertheless, the majority of them has been focused on blocks that rest at the ground level, for example Housner (1963), Yim *et al* (1980), Makris and Roussos (2000), Makris and Konstantinidis (2003), Dimitrakopoulos and DeJong (2012), Makris and Vassiliou (2013), Bachmann *et al* (2017), Bachmann *et al* (2018), Giouvanidis and Dimitrakopoulos, (2018) and Kazantzi *et al* (2021) and substantially fewer focus on contents that rest at higher floor levels, e.g. Konstantinidis and Makris (2009), Petrone *et al* (2017), Fragiadakis and Diamantopoulos (2020), in which case are subjected to floor rather than ground seismic acceleration histories. In practically all cases, pure rocking has been assumed as the predominant seismic response mechanism. This essentially implies that sufficient friction is present between the rigid block and the horizontal resting plane interface to arrest component sliding. It should be noted that sliding is a likely response mode for free-standing blocks (e.g. Lopez Garcia and Soong, 2003; Konstantinidis and Makris, 2009; Konstantinidis and Nikfar, 2015) yet its consideration remains beyond the scope of the present research.

Herein, simplified analytical expressions are offered that can be exploited by practicing design engineers and researchers for readily evaluating the seismic response statistics (i.e. the median and dispersion) of rocking-dominated (Petrone *et al*, 2017) building contents located at any floor level, other than the ground. The adopted methodology is built upon an analogous research work (Kazantzi *et al*, 2021), that was recently published by the authors, in which analytical predictive relationships for ground supported rocking blocks subjected to ordinary ground motions were proposed. To account for the filtering of the ground motion through the supporting building, we employ a set of actual horizontal floor acceleration histories recorded in instrumented buildings. The effect of vertical floor excitation on the rocking components was disregarded in view of past findings (e.g. Makris and Kampas, 2016; Linde *et al*, 2020) that it is negligible for almost all practical applications, especially when adopting a probabilistic treatment (Lachanas *et al*, 2022a).

2 BRIEF REVIEW IN THE ROCKING OSCILLATOR DYNAMICS

Our basis is the pioneering work of Housner (1963) on the rocking and overturning of free-standing blocks subjected to horizontal accelerations at their bases. Assuming that the rocking block has a rectangular shape of height $2h$ and base width $2b$ (see Figure 1) we can define a set of normalized geometrical properties for the rigid block, i.e., its stability (or slenderness) angle α, defined as,

$$\alpha = \tan^{-1}\left(\frac{b}{h}\right) \tag{1}$$

and its half diagonal R

$$R = \sqrt{b^2 + h^2} \tag{2}$$

Consequently, for a block that is subjected to a horizontal acceleration at its base, $\ddot{u}$, the equation of motion takes the following form (e.g. Vassiliou and Makris, 2013; Dar *et al*, 2016),

$$\ddot{\theta} = -p^2 \cdot \left[\sin(\alpha \cdot \mathrm{sgn}(\theta) - \theta) + \frac{\ddot{u}}{\mathrm{g}} \cdot \cos(\alpha \cdot \mathrm{sgn}(\theta) - \theta)\right] \tag{3}$$

where, sgn is the signum function, g is the acceleration of gravity, and p the characteristic frequency parameter of the rigid rocking block equal to,

$$p = \sqrt{\frac{3 \cdot g}{4 \cdot R}} \tag{4}$$

With reference to the characteristic frequency p, it should be noted that is by no means equivalent to the natural frequency of an oscillating pendulum (Makris and Konstantinidis, 2003), since the oscillation frequency strongly depends on the rocking amplitude (Housner, 1963; Yim *et al*, 1980; Makris and Konstantinidis, 2003). Yet, it is often considered a measure of the dynamic characteristics of the block, and will be used in such a manner in this study as well.

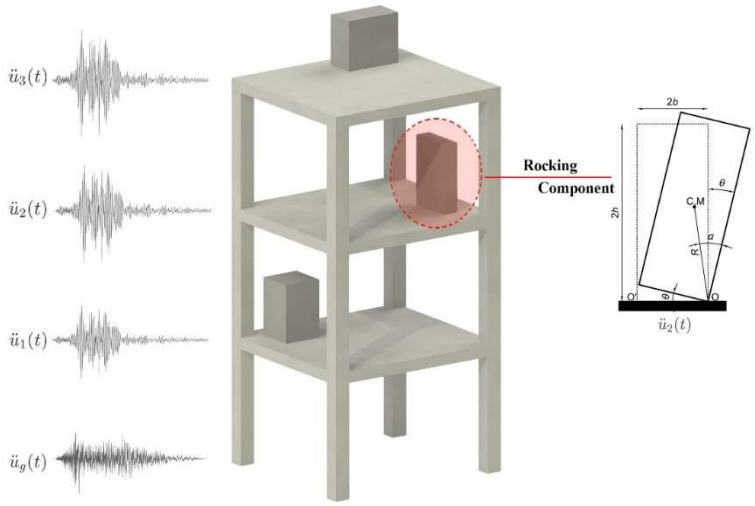

Figure 1. Generic representation of rocking components located at different floor levels and the geometry of a rocking block per Housner (1963).

Equation (3) can be solved using standard ordinary differential equation solvers. In this study the software developed by Vassiliou (2021) was employed, allowing a rapid estimation of the peak rocking angle θ_{max}. The energy losses due to impacts, have been accounted by the coefficient of restitution, η (Dimitrakopoulos and DeJong, 2012) that essentially provides a relation between the pre- and post-impact angular velocities, $\dot{\theta}_1$and $\dot{\theta}_2$, respectively, and is defined as,

$$\eta = \frac{\dot{\theta}_2}{\dot{\theta}_1} \tag{5}$$

The coefficient of restitution η typically varies between 0.7 and 1.0 (e.g. Priestley *et al*, 1978; Petrone *et al*, 2017; Ceh *et al*, 2018). On account of past observations (e.g. Bachmann *et al*, 2018; Kazantzi *et al*, 2021) that showcased the moderate effect of the restitution coefficient, as opposed to other system parameters, its randomness was disregarded herein and a typical value of $\eta = 0.92$ was assumed (e.g. Giouvanidis and Dimitrakopoulos, 2017; Kazantzi *et al*, 2021), essentially implying a total energy loss of ~15% after every impact. It should be pointed out that the adoption of this single value of the restitution coefficient is only justified on the basis of a probabilistic treatment of the rocking problem of multiple components within a building, as the one undertaken in this study, since the "true" value of η can only be experimentally determined. Its accurate estimation remains substantially important for assessing the rocking

performance of a rocking oscillator on a deterministic basis. Nevertheless, as was showcased by several past studies (e.g. Yim *et al*, 1980; Voyagaki and Vamvatsikos, 2015; Bachmann *et al*, 2017), the probabilistic seismic response assessment of rocking blocks is a robust way for effectively dealing with the high uncertainty inherent in such problems, and to the authors opinion, given the current-state-of-knowledge, the only meaningful design route.

3 SEISMIC RESPONSE EVALUATION OF ROCKING BUILDING CONTENS

The seismic response statistics of the free-standing rocking building contents, from the rocking initiation up to the overturning state, were evaluated on the basis of Incremental Dynamic Analysis (IDA, Vamvatsikos and Cornell, 2002; Lachanas and Vamvatsikos, 2022) applying as input motions at the base of the rocking blocks a suite of 105 distinct floor acceleration histories that were recorded during eight major earthquake events at the roof or the upper floors of instrumented buildings in California. In particular, the suite of floor motions was recorded in 47 buildings of variable lateral load resisting systems and heights, with the latter ranging from 2 to 52 stories. Only floor recordings producing 5% damped floor spectral acceleration ordinates higher than 0.9g were considered. It should be noted that the response in a number of the considered instrumented buildings was not restricted to the realm of linearity and several of them sustained nonnegligible damages. The strong floor accelerations that were recorded in structures that responded nonlinearly provides further evidence to an observation that was reported before by other past studies (e.g. Taghavi and Miranda, 2005) who suggested that the yielding of the primary structure is likely to have an adverse impact on the floor acceleration demands that are imparted in the building contents. More details about the characteristics of these recordings and record stations can be found in Kazantzi *et al* (2020) whereas the recorded floor acceleration histories are available from the website of the Center for Engineering Strong Motion Data (CESMD, 2018).

Floor acceleration spectra for conventional elastic oscillators often exhibit a strong narrow band amplification effect due to the filtering of the ground motion through the building, an effect that is fully captured by the utilized floor histories and cannot be discounted in any building content analysis. The decision to adopt recorded floor motions as opposed to analytical ones, essentially removes any bias associated with the latter, since the utilized input motions were recorded during real earthquakes in actual instrumented buildings. The floor acceleration histories were incrementally scaled, utilizing a constant increment of 0.01g, to obtain response estimates for the considered blocks from rocking initiation up to the block overturning, which for a rocking block signifies its collapse state. Resurrections, i.e., the appearance of stable response at intensities above the first appearance of overturning, were disregarded. This no-resurrection assumption is consistent with an acceptance of damageability of components after high energy impacts, which are typically associated with resurrections, rendering the results suitable for most practical applications, with the exception of the most durable of contents (Lachanas and Vamvatsikos, 2022).

To fully define an IDA curve, one needs an Engineering Demand Parameter (EDP) and a practical, efficient and sufficient Intensity Measure (IM, Luco and Cornell, 2007; Kazantzi and Vamvatsikos, 2015). In this study the adopted EDP was the absolute value of the peak rocking angle θ_{max} normalized by the stability angle α of the block, i.e. $\tilde{\theta} = \theta_{max}/\alpha$ (Dimitrakopoulos and Paraskeva, 2015). The onset of rocking is signified when $\tilde{\theta}$ first exceeds zero, whereas the overturning threshold is typically set to one. The overturning limit of one is a nominal threshold, yet accurate enough for the needs of this study and the limitations of the adopted analytical model, since in rare but possible cases, a rocking block could exhibit rotations higher than its stability angle without overturning. Two dimensionless IMs have been adopted, as initially proposed by Dimitrakopoulos and Paraskeva (2015), these being,

(a) the dimensionless peak floor acceleration, $PFA/(\mathrm{g}\cdot\tan\alpha)$, from this point onwards $I_A = PFA/\mathrm{g}\tan\alpha$
(b) the dimensionless peak floor velocity, $pPFV/(\mathrm{g}\cdot\tan\alpha)$, from this point onwards $I_V = pPFV/\mathrm{g}\tan\alpha$

It should be noted here that *PFA* and *PFV* exclusively refer to spectral ordinates of the single horizontal component of each floor acceleration record pair, this being the one applied to the rocking block; essentially, the arbitrary horizontal component of floor motion is employed rather than the geometric mean of both components (see Baker and Cornell, 2006). This is contrary to Kazantzi *et al* (2021), who developed expressions both for the arbitrary and the geomean component for *ground-supported* blocks. There are multiple reasons for doing so. First of all, the two components of recorded floor motions are often associated with differing periods of the supporting building as the two principal axes are rarely of identical dynamic characteristics. Perhaps not unrelated to this fact, using the arbitrary component is the overwhelming norm for all component response studies (e.g., Filiatrault and Sullivan, 2014; Kazantzi *et al*, 2020), as well. Furthermore, several instrumental recordings lack one of the two components, while in others the two components have not been measured at the same location on a floor slab. On a different tack, recognizing the uncertainty in the orientation of building contents relative to the principal axes of the supporting structure, FEMA P-58 (FEMA, 2012) typically employs the so-called "non-directional", or square-root-sum-of-squares values of *PFA* or *PFV*, while employing content fragilities based on what is essentially the arbitrary component. Following this paradigm, and given the aforementioned constraints, we also chose the arbitrary component route.

On another note, with the exception of the taller blocks (i.e. those with low *p*) close to overturning, the scaling factors for the majority of the records and blocks were kept below 2, limiting any bias due to scaling. Questions may still be raised by the fact that even such scale factors may correspond to motions that would otherwise induce nonlinearity in the structural system. Nonlinearity essentially modifies the properties of the ground motion filtering medium (i.e. the primary structure) through which the ground acceleration signal is transformed to a narrowband floor motion. Note that this is an issue regardless of whether one is investigating yielding, rocking, sliding, bouncing or any other response type. Herein, some of the utilized floor motions were recorded in instrumented buildings that deformed well beyond their elastic state, while others correspond to elastic structures. Should then the level of nonlinearity in the primary structure be adopted as an additional defining parameter in the proposed fitted relationships, or are *PFA* and *PFV* sufficient predictors of the rocking response? Actually, the lack of adequate number of strong floor motion data combined with the overall large dispersion of the rocking response does not allow us to observe any statistical trends worth mentioning. Note also that for the considerably better confined (and less dispersed case) of yielding response, NIST (2018) chose to discard any such influence in the parametric response of oscillators given *PFA*. In the same spirit, and given the data at hand, we provisionally accept sufficiency (see also Luco and Cornell, 2007) of *PFA* and *PFV* to predict rocking response, confining the influence of any nonlinearity in the supporting structure into the estimated values of *PFA* and *PFV*, rather than the response given said quantities.

4 INVESTIGATION ON FLOOR ROCKING RESPONSES

4.1 Rocking Spectra

In an analogous manner to spectral acceleration response spectra for elastic oscillators, Makris and Konstantinidis (2003) proposed the so-called rocking spectra for rocking blocks. A rocking spectrum essentially offers estimates of θ_{max} as a function of the inverse of their characteristic

frequency p (i.e. the quantity $1/p$) for different stability angles, α. Since this study is focused on components located at floor levels other than the ground, Table 1 provides a rough analogy of the quantities that appear in the rocking spectra relative to those required for defining conventional floor response spectra.

Table 1. Quantities that define floor response spectra for conventional elastic oscillators versus rocking ones.

Spectral quantity	Elastic oscillator	Rocking oscillator
component response	peak acceleration	peak rocking angle, θ_{max}
component parameters	period, T_p	inverse characteristic frequency, $1/p$
	damping ratio, β_p	slenderness/stability angle, α
building parameters	vibration period(s)	

4.2 Potential of floor rocking spectra in estimating rocking response statistics

Conventional floor response spectra evaluated for elastic oscillators exhibit large amplifications in the evaluated peak component acceleration demands in the region around the predominant period of the supporting structure. This narrowband amplification is a consequence of the ground motion filtering as the signal travels across the building height. As was showcased at least by e.g. Calvi and Sullivan (2014), Wang *et al* (2014) and Kazantzi *et al* (2020), for a vibrating component located at any floor level, the Peak Component Acceleration could be amplified by several orders of magnitude, if the period of the component is close or, even worse, tuned to the period of the supporting structure. Hence, due to this substantial amplification effect in a narrow spectral region, it was suggested by Kazantzi *et al* (2020) to perform a normalization in the abscissas of the floor response spectra (which depict the period of the component T_p) by the predominant period (fundamental or any dominant higher mode period) of the supporting structure (T_{dom}), prior to undertaking any averaging across the spectra to estimate component response statistics. This normalization process was demonstrated to be essential for maintaining in the median spectrum the peak that appears in the individual spectra at T_p/T_{dom} =1 (i.e. at tuning); median spectra obtained on the basis of unnormalized spectra could substantially underestimate the responses at and around the tuning region.

Given that floor rocking spectra may also demonstrate narrow band characteristics, normalization of their abscissas could be required prior to undertaking any statistical summarization, so as not to underestimate the responses of the rocking blocks that fall within these regions. Hence, similarly to what has been proposed in the past for the normalization of ordinary floor response spectra (Kazantzi *et al*, 2020), it was investigated herein whether there is a relation between the occurrence of spectral amplification peaks with the period of the supporting structure, and consequently whether it is meaningful to normalize the abscissas of each spectrum with such a quantity.

Figure 2 illustrates the floor rocking spectra that were computed for a range of rigid rocking blocks (with the quantity $1/p$ ranging from 0s to 2s) and two characteristic stability angles α (0.10 and 0.15 rad) for the floor acceleration recordings obtained from the 1989 Loma Prieta recording in Station 58496 and the 1991 Sierra Madre recording in Station 24385. The dashed-dot line in Figure 2 denotes the period of the supporting building, corresponding to the station designation where the floor motion history was recorded. Specifically, the rocking spectra in Figures 2a and 2b, correspond to a building with a fundamental period of

approximately 0.3s and those illustrated in Figures 2c and 2d are related to a building with a fundamental period around 0.5s.

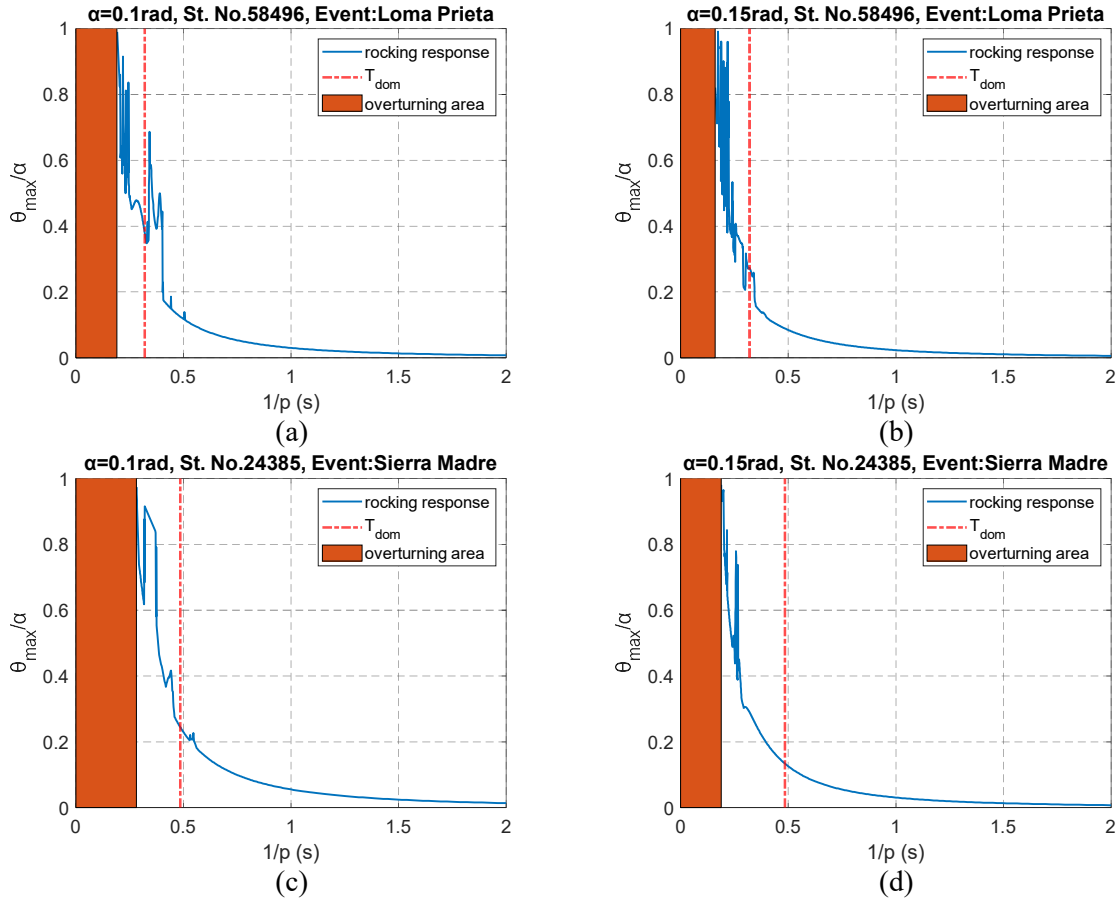

Figure 2. Floor rocking spectra for (a-b) building station 58496 and for (c-d) building station 24385 for blocks with α = 0.10 rad (left) and α = 0.15 rad (right).

As can be inferred from the Figure 2, the peak appearing in the floor rocking spectra, is nowhere close to the fundamental period of the supporting structures; similar observations also hold for all 105 floor recordings utilized in this study. Clearly, the normalization of the abscissas of the rocking spectra by the predominant period of the supporting building T_{dom} is not meaningful. Supplementary efforts towards identifying a correlation of the characteristic frequency p of the rocking blocks with the period of the supporting structure T_{dom}, via utilizing different expressions for the latter were also unsuccessful in yielding any consistent trend. Figure 3 presents more comprehensive results on two such normalization attempts compared against the unnormalized spectra and spectra normalized by T_{dom} for two indicative stability angles α (0.12 and 0.25 rad). The illustrated rocking spectra refer to eight different floor motion recordings obtained in eight different building stations, all scaled properly to the same PFV level. This moderate scaling was employed to at least ensure rocking response initiation across the considered blocks and floor motions. Apparently, none of the trial normalisation quantities of T_{dom}, $\sqrt{T_{dom}}$, or $\sqrt{t_{uni} \cdot T_{dom}}$ offered any improvement in the process of identifying any consistent interplay between the characteristic frequency p of the rocking blocks and the period of the supporting structure T_{dom}. The term t_{uni} denotes the uniform duration (Sarma and Casey,

1990; Giouvanidis and Dimitrakopoulos, 2018), evaluated as the summation of time intervals during which the floor acceleration exceeds the rocking initiation threshold $g \tan \alpha$.

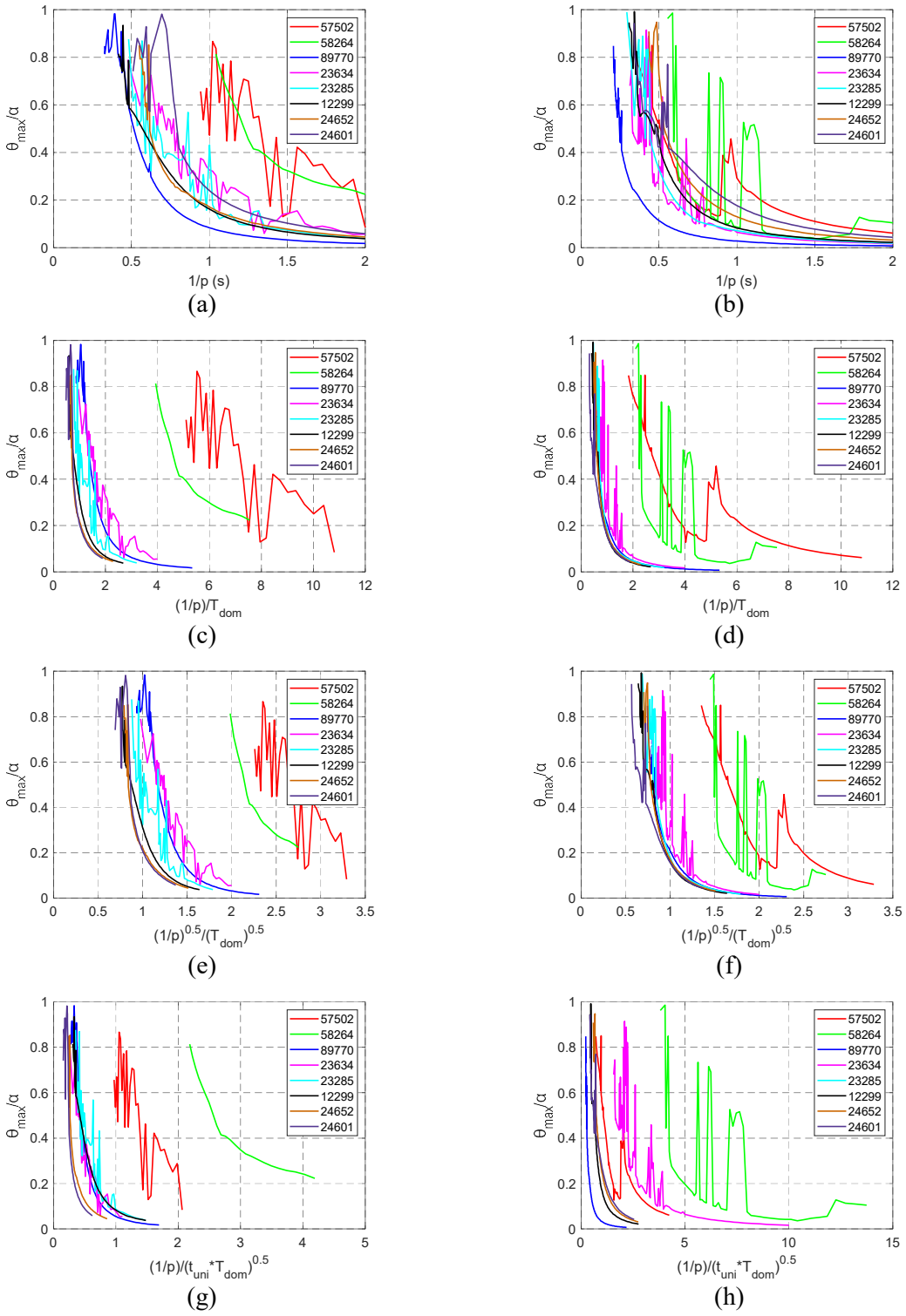

Figure 3. Floor rocking spectra for eight different building stations and α = 0.12 rad (left), α = 0.25 rad (right). The $1/p$ abscissas are shown: (a-b) unnormalized, (c-d) normalized with T_{dom}, (e-f) square rooted and normalized with $\sqrt{T_{dom}}$, and (g-h) normalized with $\sqrt{t_{uni} \cdot T_{dom}}$.

4.3 Statistical tests on floor versus ground rocking response

In subsection 4.2 it was shown that there is no apparent relationship between the characteristic frequency of a rocking building content with the fundamental period of the supporting structure. Hence, a reasonable question to be answered before we proceed with developing a set of expressions for rocking contents is whether the response of a rigid rocking block located at a floor level other than the ground (i.e. the response that is evaluated when the block is subjected to floor accelerations) is different from the response of a ground supported rigid rocking block (i.e. the response that is evaluated when the block is subjected to ground accelerations). If not, then one could utilize the rocking response prediction equations proposed on the basis of ground supported blocks (e.g. Kazantzi *et al*, 2021) for predicting the rocking responses also at different floor levels. To put it differently, the question posed is, whether, even if we were not successful in identifying the source of differentiation, floor rocking response still conforms to a different distribution than the one characterizing the ground rocking response.

To investigate this, two different suites of 105 recordings were employed. The first is the set of 105 floor recordings employed in all analyses so far, while the second pertains to the 105 ordinary (no long duration, no pulse) ground motions (not to be confused with the floor recording of the first suite) of Kazantzi *et al* (2021). From each suite, 105 values of acceleration (*PFA* or *PGA*) given $\tilde{\theta}$ were determined for a multitude of $\tilde{\theta}$ levels, covering the entire range of response from rocking initiation to overturning. In essence, vertical statistics with a median point inversion are employed, per Lachanas and Vamvatsikos (2022), in the same approach one can use to derive fragilities for exceeding given thresholds of $\tilde{\theta}$. Figure 4 presents the scatter plots of the evaluated ground (Figure 4a and 4c) and floor (Figure 4b and 4d) rocking responses for two indicative rocking blocks (with p equal to 1.0 and 2.5 s^{-1}). Apparently, there are notable differences in the evaluated ground and floor responses with reference to blocks with the same characteristic frequency whereas the dispersion observed remains nontrivial.

Then, the Kolmogorov–Smirnov (Massey, 1951; Miller, 1956) two-sample test (K–S test from this point onward) was utilized to compare the *PFA* versus the *PGA* sample determined for the same value of $\tilde{\theta}$. The K–S test is a distribution-free test, meaning that no assumption is required about the distribution of the considered data (Benjamin and Cornell, 1970). It uses the maximum absolute difference to test the null hypothesis that the two empirical cumulative distribution functions determined from the studied samples come from the same distribution given a statistical significance level, here chosen to be 5%. As can be inferred by inspecting Figure 5, there is insufficient evidence to accept the null hypothesis across the majority of $\tilde{\theta}$ responses, with results varying widely between tested blocks. Hence, there is evidence to suggest that a new model needs to be developed to capture the response of rocking blocks that are located on floor levels other than the ground.

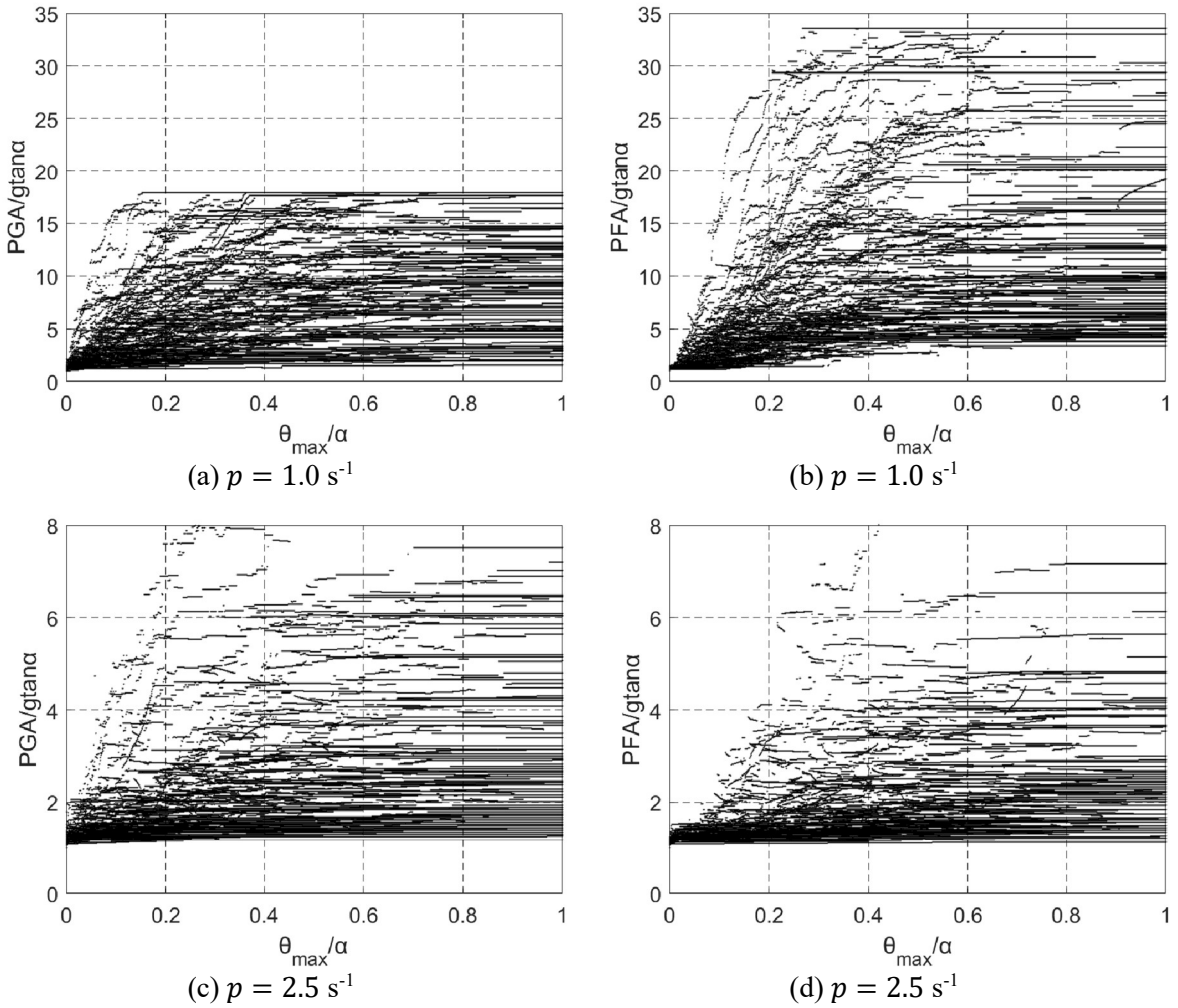

Figure 4. Scatter plots comparing the evaluated ground (a and c) and floor (b and d) rocking responses of two different blocks.

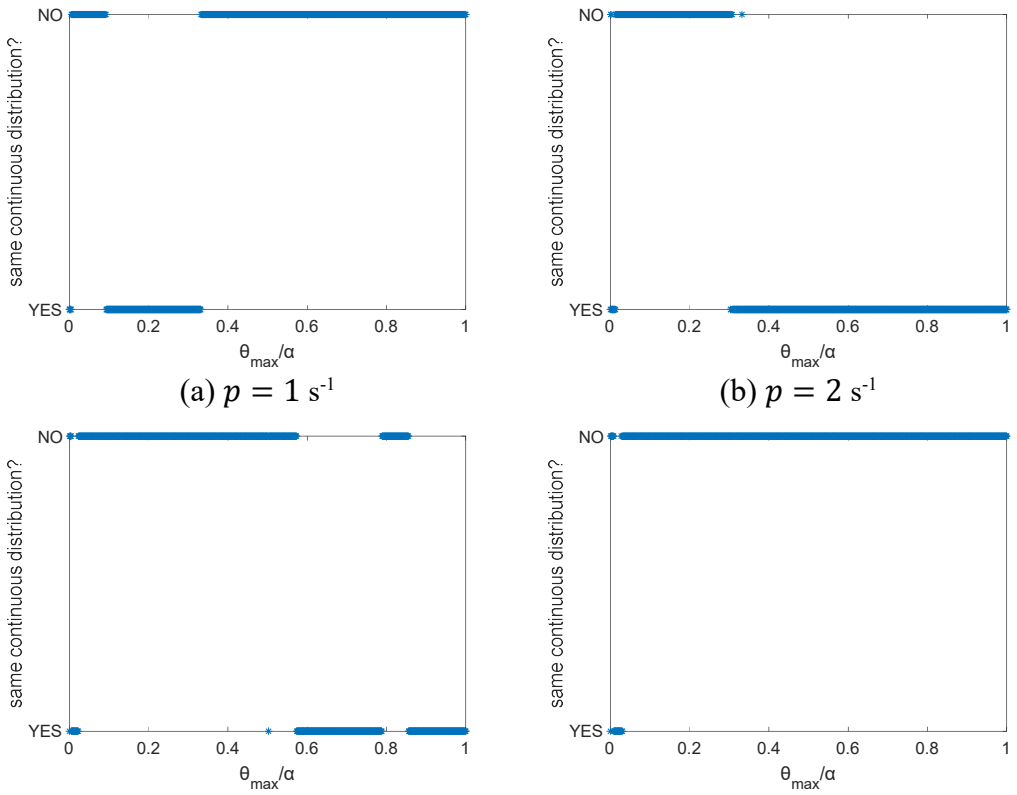

(a) $p = 1$ s^{-1} (b) $p = 2$ s^{-1}

(c) $p = 2.5$ s^{-1} (d) $p = 3.5$ s^{-1}

Figure 5. Results of K-S tests on the hypothesis that the underlying $PFA|\tilde{\theta}$ distribution is identical for ground and floor rocking response for four different blocks.

5 REGRESSION ANALYSIS ON SEISMIC DEMANDS IMPOSED TO ROCKING BUILDING CONTENTS

Owing to the observations of Section 4, we are proposing a set of equations for estimating the seismic demands of rocking building contents. They have been obtained via nonlinear regression analysis on IDA results stemming from 105 floor recordings and 41 rigid blocks with p from 1.0 up to 5.0s^{-1} and coefficient of restitution $\eta = 0.92$. Assuming a lognormal distribution of the rocking response, the proposed equations allow estimating the median and dispersion on a normalized $I - \tilde{\theta} - p$ basis, i.e., considering the absolute peak rocking rotation θ_{max} normalized by the stability angle α of the block, $\tilde{\theta} = \theta_{max}/\alpha$, and two different dimensionless IMs, I_A and I_V as defined in Section 3.1. Following the findings of Kazantzi *et al* (2021), a single value of α = 0.22 is employed, as the normalization fully removes any dependence of the statistics on α. Otherwise, the proposed equations are deemed to be valid for rigid rocking blocks within the investigated period range and having values of η not substantially different that the one adopted in this study.

5.1 Median response fitting for PFA

A two-branch equation is proposed for relating the median dimensionless *PFA* intensity (I_{A50}) with the dimensionless EDP ($\tilde{\theta}$). The first part of Equation (6a) corresponds to the rocking response domain at and around the rocking initiation. The second part provides the main median response estimates for the rocking response up to the occurrence of the first overturning:

$$I_{A50}(\tilde{\theta}) = \begin{cases} \frac{(I_{A2}-I_{A1})}{0.008} \cdot \tilde{\theta} + I_{A1}, \text{ for } 0 \le \tilde{\theta} < 0.008 \\ A_1 \cdot \left[1 - \left(1 - \tilde{\theta}^{B_1}\right)^4\right] + C_1, \text{ for } 0.008 \le \tilde{\theta} \le 1 \end{cases} \quad (6a)$$

where, I_{A2} is estimated by substituting in the second branch of Equation (6a) the value of $\tilde{\theta} = 0.008$, while A_1, B_1, C_1, and I_{A1} are parameters that can be obtained from Table 2. It should be underlined here that the proposed Equation (6a) is fully revertible since it was not obtained by means of a strict nonlinear regression process, where the statistical properties of the probability distribution are evaluated at once. Instead, the median and the dispersion of the response distribution were obtained separately, utilizing a curve fitting procedure. Hence, Equation (6a) may be inverted to obtain the median normalized peak rocking angle $\tilde{\theta}_{50}$ as a function of I_A:

$$\tilde{\theta}_{50}(I_A) = \begin{cases} 0.008 \cdot \frac{(I_A-I_{A1})}{(I_{A2}-I_{A1})}, \text{ for } I_{A1} \le I_A < I_{A2} \\ \left[1 - \left(1 - \frac{(I_A-C_1)}{A_1}\right)^{1/4}\right]^{1/B_1}, \text{ for } I_{A2} \le I_A \le (A_1 + C_1) \end{cases} \quad (6b)$$

Table 2. Parameters used with Equations (6a,b) and (7a,b) to define median values when using *PFA* and *PFV* as the IM.

IM	A_1	B_1	C_1	D_1	E_1	F_1	I_{A1} or I_{V1}
I_A i.e. $PFA/\text{gtan}\alpha$	$D_1 \cdot \exp(-E_1 \cdot p) + \frac{F_1}{p^2}$	$-0.1942 \cdot p^2 + 1.039 \cdot p + 0.5768$	$1.2700 \cdot p^{-0.066}$	36.6199	1.8213	3.6009	1.000
I_V i.e. $pPFV/\text{gtan}\alpha$	$D_1 \cdot \exp(-E_1 \cdot p) + \frac{F_1}{p^2}$	$-0.1888 \cdot p^2 + 0.8976 \cdot p + 0.7015$	$0.1366 \cdot p^{0.9345}$	2.1541	1.1144	0.3226	$0.1091 \cdot p$

As can be inferred from the plots presented in Figure 6, the proposed equation represents a good approximation of the median rocking responses for the considered range of block sizes, with its accuracy somewhat degrading for blocks having higher p values. Nonetheless, given the inherent uncertainty of the problem at hand but also to maintain the practicality and the invertibility of the proposed Equation (6a) we refrained from its further refinement. Further to the above, one notable observation (more apparent in Figure 6b due to the narrower range of the vertical axis compared to that of Figure 6a) is the trend change in the evaluated rocking responses that occurs at a $PFA/\text{gtan}\alpha$ level that is approximately equal to 1.3 (i.e. 30% greater compared to the rocking initiation threshold). For the blocks examined in the present study, it was revealed that rocking response increases at a higher rate for low floor acceleration demands ($PFA/\text{gtan}\alpha$ <1.3) as well as close to overturning. This echoes the observations of Dimitrakopoulos and Paraskeva (2015) who identified the same approximate transition threshold for rocking blocks subjected to near-field ground motion records.

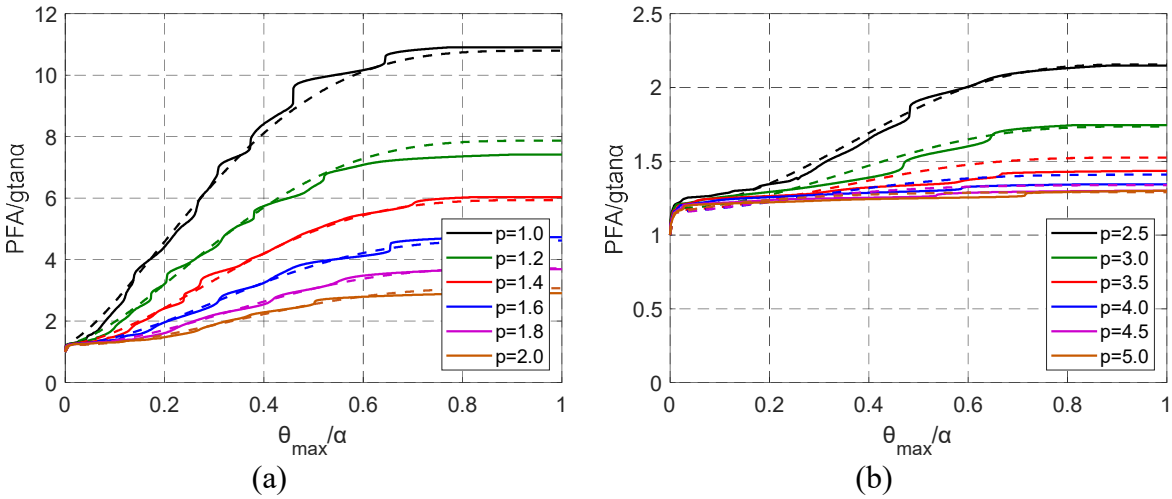

Figure 6. Median seismic demand estimates for rocking building contents with different characteristic frequencies p over a range of intensity levels, expressed in terms of dimensionless *PFA*, covering the response from rocking initiation up to the first overturning. Fitting is shown with the dashed line.

5.2 Median response fitting for PFV

In an analogous manner to the process adopted in the case of *PFA*s, a similar methodology was utilized for delivering an equation that relates the median dimensionless *PFV* intensity measure (I_{V50}) with the dimensionless EDP ($\tilde{\theta}$). Hence, similarly to Equation (6a), the first part of Equation (7a) corresponds to the rocking response domain at and around the rocking initiation whereas the second part provides the main median response estimates for the rocking response up to the occurrence of the first overturning:

$$I_{V50}(\tilde{\theta}) = \begin{cases} \frac{(I_{V2}-I_{V1})}{0.004} \cdot \tilde{\theta} + I_{V1}, \text{ for } 0 \le \tilde{\theta} < 0.004 \\ A_1 \cdot \left[1 - \left(1 - \tilde{\theta}^{B_1}\right)^4\right] + C_1, \text{ for } 0.004 \le \tilde{\theta} \le 1 \end{cases} \quad (7a)$$

where, I_{V2} is estimated by substituting in the second branch of Equation (7a) the value of $\tilde{\theta} = 0.004$, while A_1, B_1, C_1 and I_{V1} are provided in Table 2. For reasons explained in Section 5.1, Equation (7a) may be inverted to obtain the median normalized peak rocking angle $\tilde{\theta}_{50}$ as a function of I_V:

$$\tilde{\theta}_{50}(I_V) = \begin{cases} 0.004 \cdot \frac{(I_V-I_{V1})}{(I_{V2}-I_{V1})}, \text{ for } I_{V1} \le I_V < I_{V2} \\ \left[1 - \left(1 - \frac{(I_V-C_1)}{A_1}\right)^{1/4}\right]^{1/B_1}, \text{ for } I_{V2} \le I_V \le (A_1 + C_1) \end{cases} \quad (6b)$$

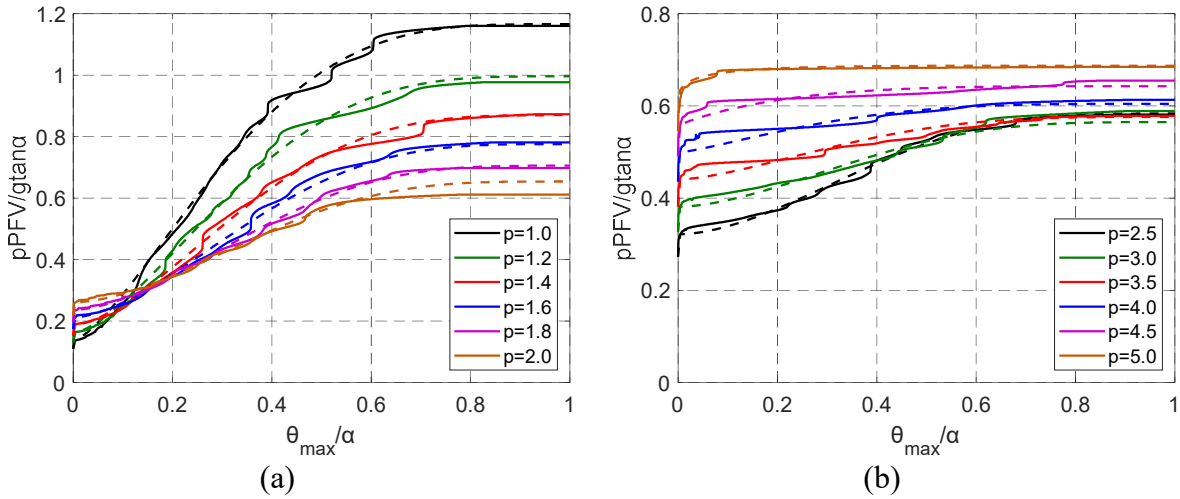

(a) (b)

Figure 7. Median seismic demand estimates for rocking building contents with different characteristic frequencies p over a range of intensity levels, expressed in terms of dimensionless *PFV*, covering the response from rocking initiation up to the first overturning. Fitting is shown with the dashed line.

5.3 Dispersion fitting for PFA

To offer a comprehensive probabilistic description for the seismic rocking response of building contents, along with the median equations, another set is needed for providing dispersion estimates. Hence, similarly to the process adopted for delivering the median fitting, a nonlinear regression analysis was undertaken on the standard deviations of the data logarithms, in view that the seismic response is sufficiently described by means of a lognormal distribution. As in the case of the medians, the curve fitting process resulted in a two-part expression that offers dispersion estimates for I_A as a function of p:

$$\beta_A(\tilde{\theta}) = \begin{cases} \frac{A_2 \cdot \tilde{\theta}^{0.6}}{\exp(\tilde{\theta})} - \frac{B_2 \cdot \tilde{\theta}}{\exp(C_2 \cdot \tilde{\theta})}, & \text{for } \tilde{\theta} \le 0.7 \\ \beta_A(\tilde{\theta} = 0.7), & \text{elsewhere} \end{cases} \tag{8}$$

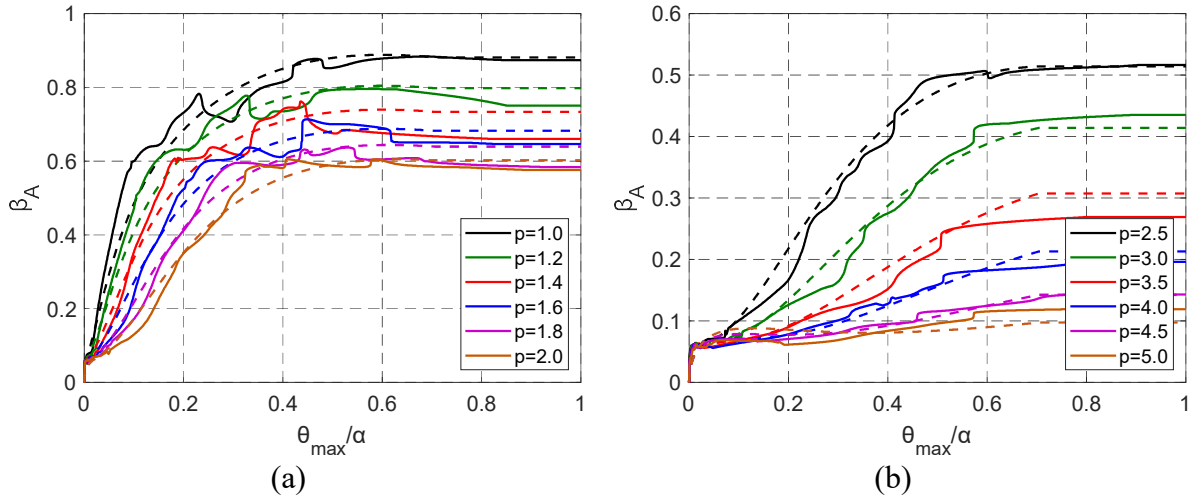

(a) (b)

Figure 8. *PFA* dispersion estimates for rocking building contents with different characteristic frequencies p over a range of imposed demands, from rocking initiation up to the first overturning. Fitting is shown with the dashed line.

As can be inferred by inspecting both Equation (8) and Figure 8, at the initiation of rocking the dispersion is zero, since the initiation of rocking occurs at $I_A = 1$ irrespectively of the block characteristic frequency. Hence, at low seismic demands, i.e. at and around the rocking initiation, the normalized *PFA* is a very efficient IM, i.e. one that possesses a high correlation with the rocking response. Nevertheless, its efficiency decreases rapidly for $\tilde{\theta}$ values that are higher than 0.3, or even 0.2; for the largest blocks considered in this study (Figure 8a) it stabilizes at fairly large dispersions when $\tilde{\theta}$ reaches 0.7, with the maximum reported value being around 0.9 for the block with $p = 1s^{-1}$. These observations essentially render I_A a rather inefficient IM for large blocks when considering high responses that could induce severe damage to these components. For smaller components (i.e. $p > 2.5s^{-1}$, see Figure 8b), which are of more practical interest to the majority of building contents, the dispersions take more reasonable values, of the order of 0.1 to 0.5.

Table 3. Parameters used with Equations (8) and (9) to define dispersion values when using *PFA* and *PFV* as the IM.

IM	A_2	B_2	C_2
I_A i.e. $PFA/\text{gtan}\alpha$	$2.1991 \cdot p^{-0.544}$	$10.9120 \cdot e^{-0.402 \cdot p}$	$38.6370 \cdot p^{-1.871}$
I_V i.e. $pPFV/\text{gtan}\alpha$	$-0.0396 \cdot p^3 + 0.4827 \cdot p^2 - 1.9095 \cdot p + 2.4904$	$663.2170 \cdot p^{-4.316}$	$48.8860 \cdot p^{-2.008}$

5.4 Dispersion fitting for *PFV*

Similarly to the previous subsection, the nonlinear regression analysis on the dispersion estimates for *PFV* used as an IM yield the following two-part expression that offers dispersion estimates for I_V as a function of p:

$$\beta_V(\tilde{\theta}) = \begin{cases} \frac{A_2 \cdot \tilde{\theta}^{0.8}}{\exp(\tilde{\theta})} - \frac{B_2 \cdot \tilde{\theta}^2}{\exp(C_2 \cdot \tilde{\theta})} + 0.2853, & \text{for } \tilde{\theta} \le 0.6 \\ \beta_V(\tilde{\theta} = 0.6), & \text{elsewhere} \end{cases} \quad (9)$$

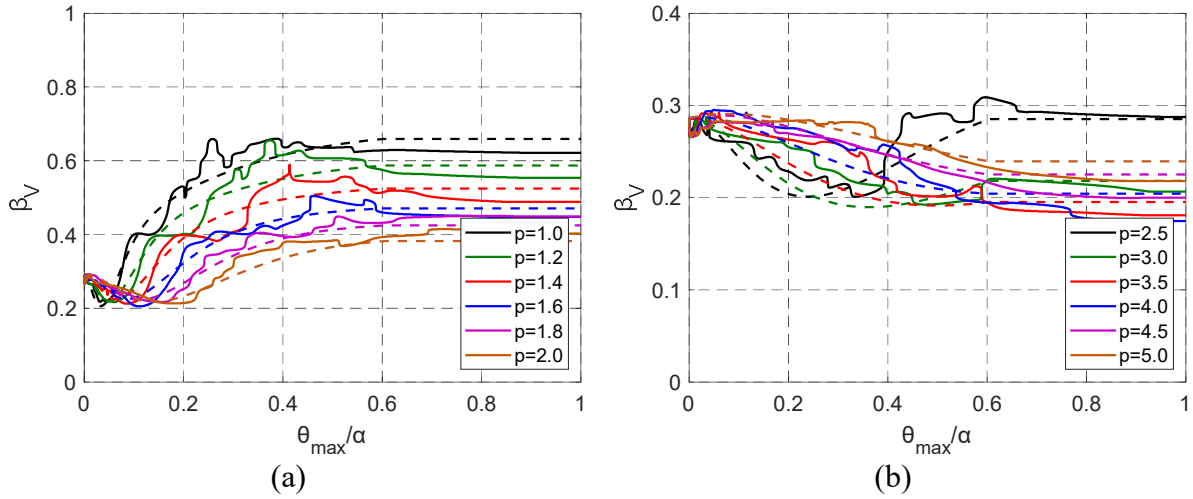

Figure 9. *PFV* dispersion estimates for rocking building contents with different characteristic frequencies p over a range of imposed demands, from rocking initiation up to the first overturning. Fitting is shown with the dashed line.

By inspecting Figure 9, I_V is a more efficient IM compared to I_A for most of the range of response and most of the blocks. The only exceptions are the neighborhood of initial rocking uplift (i.e., $\tilde{\theta} \leq 0.2$) and the smaller components (i.e. $p > 3.5s^{-1}$, see Figure 9b), where I_A performs better. These two observations are actually well correlated, as the smaller blocks are also less stable (e.g., Makris and Kampas, 2016), rapidly reaching overturning at intensities close to the initiation of rocking uplift. The aforementioned findings are believed to hold at least for the size range of the floor contents that was considered in this study, as far as those are consistently exhibiting pure rocking behavior during the seismic excitation.

6 CASE STUDY

As an example, the equations presented in Section 5 are applied to two arbitrary components, namely A and B (see Table 4), to evaluate their fragility. Three sequential limit states are employed, defined via two deterministic thresholds for the normalized peak rocking angle $\tilde{\theta}$ (i.e. 0.15 and 0.35), to roughly depict damage initiation and moderate damage for a typical component, whereas a third threshold of 1.0 is associated with nominal overturning. It should be noted that the nature of the component (e.g. rugged electronic equipment versus fragile museum artefact) essentially defines these thresholds; the values adopted are only indicative.

Table 4. Geometric properties of the considered case-study rocking components.

Component	$2h$	$2b$	R	p	α
Component A	2.307	0.468	1.177	2.5	0.20
Component B	1.164	0.297	0.601	3.5	0.25

The component fragilities were evaluated on the basis of a lognormal distribution assumption for the fragility (Bakalis and Vamvatsikos, 2018) as,

$$P(Demand > Capacity|I) = \Phi\left(\frac{\ln(I)-\ln(I_{50})}{\beta}\right) \quad (10)$$

where I is the dimensionless IM (i.e. I_A or I_V), I_{50} its median computed using either Equation (6a) or (7a), and β its dispersion (i.e. β_A or β_V) evaluated utilizing Equation (8) or (9). The median and the dispersion of the component fragilities, considering both dimensionless IMs, components A-B, and the three limit states, are summarized in Table 5.

Figure 10 illustrates the corresponding fragility curves for I_A (Figure 10a,c) and I_V (Figure 10b,d). The essential determinism of rocking initiation at $I_A = 1$ is slightly violated, as the lognormal distribution model predicts low, but still non-zero rocking response even for *PFA*s below the rocking initiation threshold of $I_A < 1$. Subsequently, it is no wonder that the order of the fragilities is scrambled in that problematic region, as more severe damage states may appear to be more probable than milder ones at given IMs in this region. This can be partially attributed to the low efficiency of *PFA*, which manifests itself by high dispersion values as the rocking response deviates from the rocking initiation region. Due to this effect, the approximation of the fragility with a two-parameter lognormal distribution, which is further always bounded to the origin regardless of the response level, could have an adverse impact on the computed probabilities in the neighborhood of initial uplift. In case of a risk assessment, the aforementioned limitation of the two-parameter lognormal distribution could have a substantial impact on the evaluated annual exceedance probability. Different distributions may be considered to improve the probabilistic quantification, e.g. by utilizing a shifted three-parameter lognormal distribution (e.g. Stoica *et al*, 2007). An even simpler approach is to cut-off the left tail of the lognormal fragility (e.g. Lachanas *et al*, 2022b), zeroing it out for $I_A < 1$. Nevertheless, it is out of the scope of this study to further elaborate on this issue. It should be noted that the fragilities evaluated utilizing I_V as an IM do not appear to have such issues. This

is due to the fact that the dispersions at higher response levels are low, while *PFV* is not as efficient for rocking initiation, leaving some non-zero dispersion in that neighborhood to allow for better lognormal fitting.

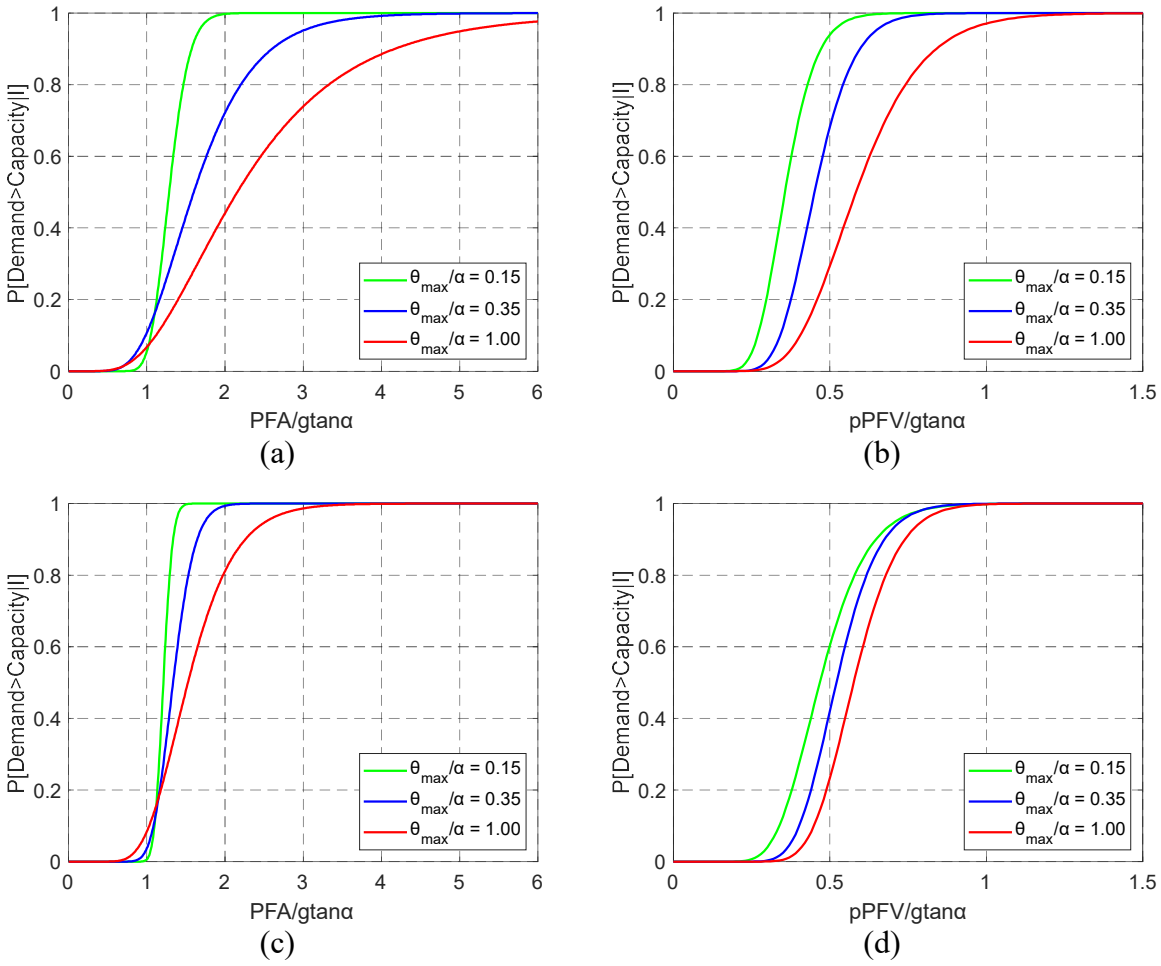

Figure 10. Median fragility curves computed for three sequential damage states using the proposed equations (see Table 5) for Component A (a-b) and Component B (c-d) expressed in terms of the normalized *PFA*s (a and c) and *PFV*s (b and d).

Table 5. *PFA* and *PFV* fragility estimates for the three considered limit states

Component	$\tilde{\theta} = 0.15$		$\tilde{\theta} = 0.35$		$\tilde{\theta} = 1.00$	
	I_{A50} [(a)]	β_A [(b)]	I_{A50}	β_A	I_{A50}	β_A
Component A	1.29	0.16	1.60	0.38	2.16	0.51
Component B	1.21	0.08	1.34	0.16	1.53	0.31
	I_{V50} [(c)]	β_V [(d)]	I_{V50}	β_V	I_{V50}	β_V
Component A	0.36	0.22	0.45	0.22	0.58	0.28
Component B	0.47	0.25	0.52	0.20	0.58	0.20

[(a)] Equation (6a), [(b)] Equation (8)
[(c)] Equation (7a), [(d)] Equation (9)

In subsection 4.3 it was showcased that the ground and floor rocking responses come from different distributions. To further expand on this finding and demonstrate the error that could be induced in a risk assessment if one ignores this observation, it was also checked, for a

sample rocking block (Component A), whether utilizing the proposed equations obtained on the basis of floor acceleration histories yields substantially different fragility estimates for the building contents than those computed by means of similar equations obtained for the ground. To accomplish this comparison, an additional set of fragilities for the same three damage states presented in Figure 10 and considering the properties of Component A, were evaluated utilizing the *PGA* regression equations proposed for ground-supported rocking components by Kazantzi *et al* (2021). Having the two fragilities sets at hand, it was also assumed that the considered component may be located at two different buildings, having fundamental periods of 0.5s and 2.0s, respectively, and subjected to a *PGA* = 0.2g. In the absence of more elaborate data, one may evaluate the resulting floor accelerations by means of the following *PFA*/*PGA* relationship suggested by NIST (2018),

$$\left(\frac{PFA}{PGA}\right) = 1 + a_1 \cdot \left(\frac{z}{H}\right) + a_2 \cdot \left(\frac{z}{H}\right)^{10} \tag{11}$$

where,

$$a_1 = \frac{1}{T_{blg}} \leq 2.5 \tag{12}$$

$$a_2 = \left[1 - \left(\frac{0.4}{T_{blg}}\right)^2\right] > 0 \tag{13}$$

T_{blg} is the period of the supporting building that is suggested to be evaluated per ASCE/SEI 7-16; z is the vertical location of the component measured from the ground and H is the building height.

For the two considered buildings and four different elevations of z/H = 0.25, 0.50, 0.75 and 1, Equation (11) yields the *PFA* estimates presented in the second column of Table 6. As can be inferred from the tabulated values, for the same level of floor acceleration, utilizing the ground-based relationships yields lower exceedance probability estimates for all combinations of blocks, buildings and limit states. This further supports a recent finding by D'Angela *et al* (2021) suggesting that floor motions are in general more severe than ground motions. Also, by inspecting the fragility curves presented in Figure 11 it is further verified that the floor-acceleration-based fragilities and the ground-acceleration-based fragilities indicate two different distributions of rocking response by having different medians and dispersions.

Now the question turns to whether this difference is justifiable at all floors within the building. First, it should be pointed out that the 105 floor acceleration recordings were mainly obtained from the top of the building. Hence, they are certainty representative of floor motion at the upper floors, yet some doubts may be raised as to whether they offer accurate representation for lower floors. In general, it is well known that the upper floor response is better tuned to the fundamental period of the structure, while lower ones often show more influence by higher modes. When developing predictive relationships for simple oscillators (e.g., Kazantzi *et al*, 2020), it is the normalization by a characteristic supporting-structure period that allows one to claim wider legitimacy of the fitted expressions. Herein, where no such normalization could be found, how is one to still claim validity of Equations (6)–(9) for floors that were not investigated? There are two answers to this. First, the lack of any dependence on a particular modal period offers at least some evidence to support that the specifics of the narrowband content of floor motion are not as important for rocking systems. Second, even if some dependence cannot be ruled out, the *PFA*-based fragility estimates will at worst offer a conservative estimation even for the lowest of floors. This is in line with the typical practice of designing components for the worst *PFA* to be encountered in the structure, i.e., which for the majority of the buildings occurs at or close to the roof. On the other hand, using the *PGA*-based fragilities (essentially assuming the supporting structure is rigid) will surely result to underestimation of damage and loss, especially for building contents located at the top of building.

Table 6. Exceedance probability estimates for the three considered limit states obtained for Component A located in buildings with fundamental periods of 0.5s and 2.0s. The values shown in roman font are derived from Equations (6a) and (8), while those in bold are based on *PGA*-based regression equations of Kazantzi *et al* (2021).

T_{blg} = 0.50 s		$P[\tilde{\theta} > \tilde{\theta}_c \mid PFA]$					
z/h	*PFA* (g)	$\tilde{\theta}_c = 0.15$		$\tilde{\theta}_c = 0.35$		$\tilde{\theta}_c = 1.00$	
0.25	0.30	0.81	**0.45**	0.42	**0.28**	0.23	**0.17**
0.50	0.40	1.00	**0.81**	0.71	**0.52**	0.43	**0.33**
0.75	0.50	1.00	**0.95**	0.88	**0.71**	0.61	**0.49**
1.00	0.67	1.00	**1.00**	0.97	**0.88**	0.80	**0.68**
T_{blg} = 2.00 s		$P[\tilde{\theta} > \tilde{\theta}_c \mid PFA]$					
z/h	*PFA* (g)	$\tilde{\theta}_c = 0.15$		$\tilde{\theta}_c = 0.35$		$\tilde{\theta}_c = 1.00$	
0.25	0.22	0.18	**0.13**	0.17	**0.12**	0.10	**0.07**
0.50	0.25	0.39	**0.22**	0.25	**0.17**	0.14	**0.10**
0.75	0.28	0.72	**0.38**	0.37	**0.25**	0.20	**0.15**
1.00	0.49	1.00	**0.94**	0.86	**0.69**	0.59	**0.47**

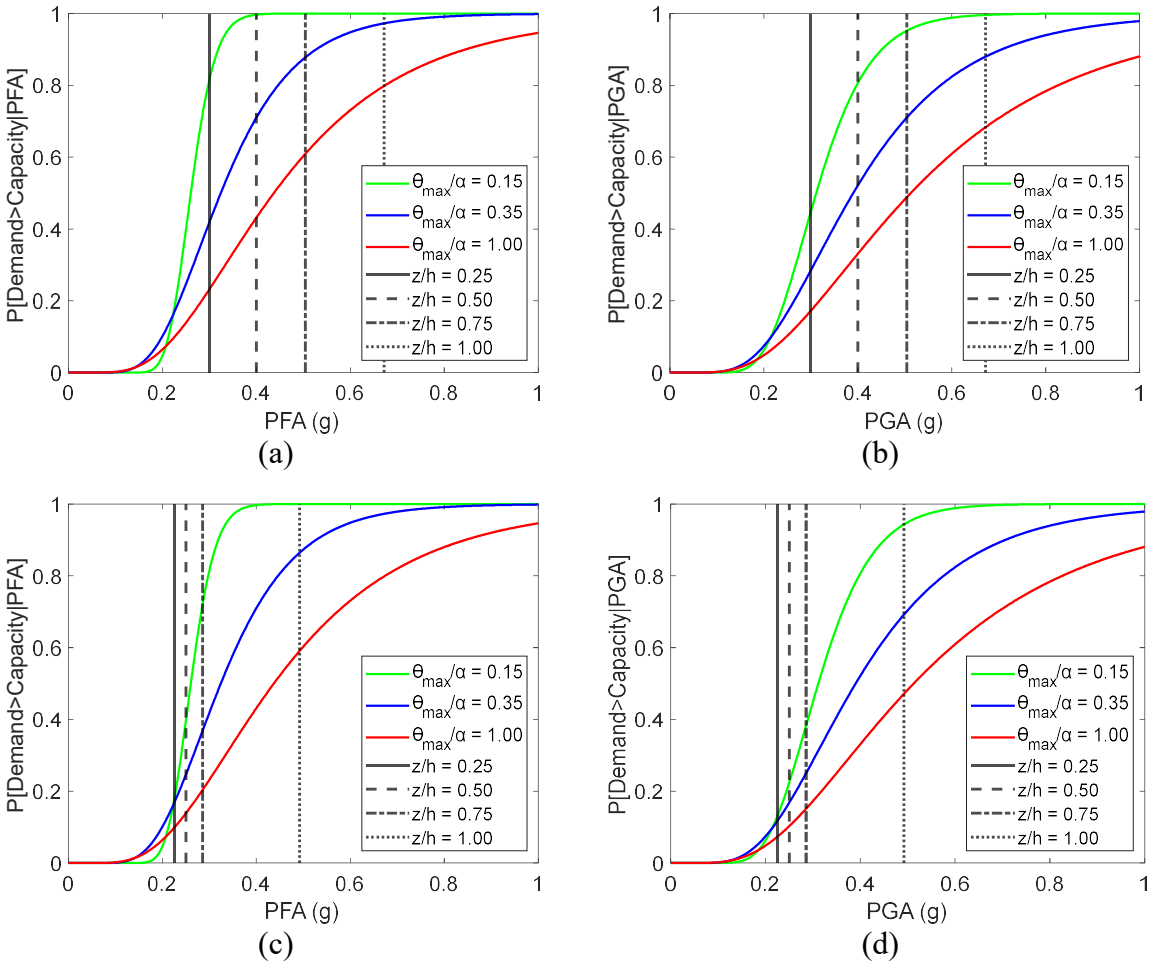

Figure 11. Median fragility curves computed in three sequential damage states using the *PFA*-based equations (i.e., incorporating the influence of supporting structure flexibility) and the *PGA*-based equations (i.e., assuming a rigid supporting structure) for Component A located in two supporting buildings with periods (a-b) T_{blg} = 0.5s and (c-d) T_{blg} = 2.0s.

CONCLUSIONS

The present study offers a practical method for determining the response statistics for a spectrum of rocking block sizes, through a set of equations obtained via nonlinear regression on their analytically computed seismic responses. The method employs analytically derived rocking response data having subjected several rocking block models to multiple floor recordings. The latter are actual floor acceleration histories that were obtained from instrumented buildings in California during real earthquakes. The floor recordings were incrementally scaled so as to expose the entire response performance of a rocking block that essentially spans across rocking initiation and block overturning. The resulting normalized $I - \tilde{\theta} - p$ expressions offer a practical design and assessment tool that can be utilized for delivering more stable free-standing nonstructural building contents and consequently minimizing the pertinent seismic losses. Finally, the analyses also revealed that I_V is a more efficient intensity measure than I_A away from the rocking initiation region and for the majority of the block sizes.

ACKNOWLEDGEMENTS

The authors would like to thank Dr. M. Vassiliou for providing the software for undertaking the numerical study on the rocking oscillators under earthquake excitations and Ms. E. Vourlakou for preparing the photorealistic image of the supporting building. We also acknowledge the constructive criticism of the two anonymous reviewers who helped improve the manuscript.

REFERENCES

Bachmann JA, Strand M, Vassiliou MF, Broccardo M, Stojadinović B. Is rocking motion predictable? Earthquake *Engineering and Structural Dynamics*, 47(2):535–552, 2018. https://doi.org/10.1002/eqe.2978

Bachmann JA, Vassiliou MF, Stojadinović B. Dynamics of rocking podium structures. *Earthquake Engineering and Structural Dynamics*, 46: 2499–2517, 2017. https://doi.org/10.1002/eqe.2915

Bakalis K, Vamvatsikos D. Seismic fragility functions via nonlinear response history analysis. *Journal of Structural Engineering (ASCE)*, 144(10):04018181, 2018. https://doi.org/10.1061/(ASCE)ST.1943-541X.0002141

Baker JW, Cornell CA. Which spectral acceleration are you using? *Earthquake Spectra*, 22(2):293–312, 2006. https://doi.org/10.1193/1.2191540

Benjamin JR, Cornell CA. Probability, statistics, and decision for civil engineers. McGraw-Hill, 1970.

Calvi P, Sullivan TJ. Estimating floor spectra in multiple degree of freedom systems. *Earthquakes and Structures*, 7(1): 12–38, 2014. http://dx.doi.org/10.12989/eas.2014.7.1.017

Ceh N, Jelenic G, Bicanic N. Analysis of restitution in rocking of single rigid blocks. *Acta Mechanica*, 229: 4623–4642, 2018. https://doi.org/10.1007/s00707-018-2246-8

CESMD (Center for Engineering Strong Motion Data). Data for latest earthquakes: available at http://www.strongmotioncenter.org, last accessed May 2018.

Dar A, Konstantinidis D, El-Dakhakhni WW. Evaluation of ASCE 43-05 seismic design criteria for rocking objects in nuclear facilities. *Journal of Structural Engineering (ASCE)*, 142(11): 04016110, 2016. https://doi.org/10.1061/(ASCE)ST.1943-541X.0001581

D'Angela D, Magliulo G, Cosenza E. Seismic damage assessment of unanchored nonstructural components taking into account the building response. Structural Safety, 93: 102126, 2021. https://doi.org/10.1016/j.strusafe.2021.102126

Dimitrakopoulos EG, DeJong MJ. Revisiting the rocking block: closed-form solutions and similarity laws. *Proceedings of the Royal Society A: Mathematical, Physical and Engineering Sciences*, 468(2144): 2294–2318, 2012. https://doi.org/10.1098/rspa.2012.0026
Dimitrakopoulos EG, Paraskeva TS. Dimensionless fragility curves for rocking response to near-fault excitations. *Earthquake Engineering and Structural Dynamics*, 44(12):2015–2033, 2015. https://doi.org/10.1002/eqe.2571
FEMA. FEMA 356 - Prestandard and commentary for the seismic rehabilitation of buildings, Federal Emergency Management Agency, 2000.
FEMA. Seismic Performance Assessment of Buildings, Applied Technology Council for the Federal Emergency Management Agency, Washington, DC, Report No. FEMA P-58, 2012.
Filiatrault A, Sullivan T. Performance-based seismic design of nonstructural building components: The next frontier of earthquake engineering. *Earthquake Engineering and Engineering Vibration*, 13 (S1): 17–46, 2014. https://doi.org/10.1007/s11803-014-0238-9
Fragiadakis M, Diamantopoulos S. Fragility and risk assessment of freestanding building contents. *Earthquake Engineering and Structural Dynamics*, 49(10): 1028–1048, 2020. https://doi.org/10.1002/eqe.3276
Giouvanidis AI, Dimitrakopoulos EG. Seismic performance of rocking frames with flag-shaped hysteretic behavior. *Journal of Engineering Mechanics (ASCE)*, 143(5): 04017008, 2017. https://doi.org/10.1061/(ASCE)EM.1943-7889.0001206
Giouvanidis AI, Dimitrakopoulos EG. Rocking amplification and strong motion duration. *Earthquake Engineering and Structural Dynamics*, 47(10): 2094–2116, 2018. https://doi.org/10.1002/eqe.3058
Housner GW. The behavior of inverted pendulum structures during earthquakes. *Bulletin of the Seismological Society of America*, 53(2): 403–417, 1963.
Kazantzi AK, Lachanas CG, Vamvatsikos D. Seismic response distribution expressions for on-ground rigid rocking blocks under ordinary ground motions. *Earthquake Engineering and Structural Dynamics*, 50(12): 3311–3331, 2021. https://doi.org/10.1002/eqe.3511
Kazantzi AK, Vamvatsikos D. Intensity measure selection for vulnerability studies of building classes. *Earthquake Engineering and Structural Dynamics*, 44(15): 2677–2694, 2015. https://doi.org/10.1002/eqe.2603
Kazantzi AK, Vamvatsikos D, Miranda E. Evaluation of seismic acceleration demands on building nonstructural elements. *Journal of Structural Engineering (ASCE)*, 146(7): 04020118, 2020. https://doi.org/10.1061/(ASCE)ST.1943-541X.0002676
Konstantinidis D, Makris N. Experimental and analytical studies on the response of freestanding laboratory equipment to earthquake shaking. *Earthquake Engineering and Structural Dynamics*, 38(6): 827–848, 2009. https://doi.org/10.1002/eqe.871
Konstantinidis D, Nikfar F. Seismic response of sliding equipment and contents in base-isolated buildings subjected to broadband ground motions. *Earthquake Engineering and Structural Dynamics*, 44:865–887, 2015. https://doi.org/10.1002/eqe.2490
Lachanas CG, Vamvatsikos D. Rocking incremental dynamic analysis. *Earthquake Engineering and Structural Dynamics*, 51(3):688–703, 2022. https://doi.org/10.1002/eqe.3586
Lachanas CG, Vamvatsikos D, Vassiliou MF. The influence of the vertical component of ground motion on the probabilistic treatment of the rocking response of free-standing blocks. *Earthquake Engineering and Structural Dynamics*, 2022a. https://doi.org/10.1002/eqe.3643
Lachanas C.G., Melissianos V.E., Vamvatsikos D. Spatial Variability of Ground Motion Hazard and Preliminary Regional Damage Assessment of Ancient Monuments. In: Vayas I., Mazzolani F.M. (eds) Protection of Historical Constructions. PROHITECH 2021. Lecture Notes in Civil Engineering, vol 209. Springer, Cham, 2022b. https://doi.org/10.1007/978-3-030-90788-4_49

Linde SA, Konstantinidis D, Tait MJ. Rocking response of unanchored building contents considering horizontal and vertical excitation. *Journal of Structural Engineering (ASCE)*, 146(9): 04020175-1, 2020. https://doi.org/10.1061/(ASCE)ST.1943-541X.0002735
Lopez Garcia D, Soong TT. Sliding fragility of block-type non-structural components. Part 1: unrestrained components. *Earthquake Engineering and Structural Dynamics*, 32(1):111–129, 2003. https://doi.org/10.1002/eqe.217
Luco N, Cornell CA. Structure-specific scalar intensity measures for near-source and ordinary earthquake ground motions. *Earthquake Spectra*, 23(2): 357–392, 2007. https://doi.org/10.1193/1.2723158
Makris N, Kampas G. Size Versus Slenderness: Two Competing Parameters in the Seismic Stability of Free-Standing Rocking Columns. *Bulletin of the Seismological Society of America*,106(1):104–122, 2016. http://dx.doi.org/10.1785/0120150138
Makris N, Konstantinidis D. The rocking spectrum and the limitations of practical design methodologies. *Earthquake Engineering and Structural Dynamics*, 32(2): 265–289, 2003. https://doi.org/10.1002/eqe.223
Makris N, Roussos Y. Rocking response of rigid blocks under near-source ground motions. *Géotechnique*, 50(3): 243–262, 2000. https://doi.org/10.1680/geot.2000.50.3.243
Makris N, Vassiliou MF. Planar rocking response and stability analysis of an array of free-standing columns capped with a freely supported rigid beam. *Earthquake Engineering and Structural Dynamics*, 42(3):431–449, 2013. https://doi.org/10.1002/eqe.2222
Massey FJ. The Kolmogorov-Smirnov test for goodness of fit. *Journal of the American Statistical Association*, 46(253): 68–78, 1951.
Miller LH. Table of percentage points of Kolmogorov statistics. *Journal of the American Statistical Association*, 51(273): 111–121, 1956.
National Institute of Standards and Technology (NIST). NIST GCR 18-917-43 Report: Recommendations for Improved Seismic Performance of Nonstructural Components, 2018. https://doi.org/10.6028/NIST.GCR.18-917-43
Parisi F, Augenti N. Earthquake damages to cultural heritage constructions and simplified assessment of artworks. *Engineering Failure Analysis*, 34: 735–760, 2013. https://doi.org/10.1016/j.engfailanal.2013.01.005
Petrone C, Di Sarno L, Magliulo G, Cosenza E. Numerical modelling and fragility assessment of typical freestanding building contents. *Bulletin of Earthquake Engineering*, 15: 1609–1633, 2017. https://doi.org/10.1007/s10518-016-0034-1
Priestley MJN, Evison RJ, Carr AJ. Seismic response of structures free to rock on their foundations. *Bulletin of the New Zealand National Society for Earthquake Engineering*, 11(3): 141–150, 1978.
Sarma SK, Casey BJ. Duration of strong motion in earthquakes. In: Proceedings of the 9th European Conference on Earthquake Engineering, Moscow, Russia, pp.174–183, 1990.
Spyrakos CC, Maniatakis CA, Taflampas IM. Application of predictive models to assess failure of museum artifacts under seismic loads. *Journal of Cultural Heritage*, 23(1):11–21, 2017. https://doi.org/10.1016/j.culher.2016.10.001
Stoica M, Medina RA, McCuen RH. Improved probabilistic quantification of drift demands for seismic evaluation, Structural Safety, 29(2):132–145, 2007. https://doi.org/10.1016/j.strusafe.2006.03.003
Taghavi S, Miranda E. Response assessment of nonstructural building elements. PEER Rep. No. 2003/05. Berkeley, CA: Univ. of California Berkeley, 2005.
Vamvatsikos D, Cornell CA. Incremental dynamic analysis. *Earthquake Engineering and Structural Dynamics*, 31(3):491–514, 2002. https://doi.org/10.1002/eqe.141
Vassiliou MF. Rocking response of a rigid block to a ground motion, MATLAB script: available at https://n.ethz.ch/~mvassili/scripts.html, last accessed September 2021.

Makris N, Vassiliou MF. Planar rocking response and stability analysis of an array of free-standing columns capped with a freely supported rigid beam. *Earthquake Engineering and Structural Dynamics*, 42 (3): 431–449, 2013. https://doi.org/10.1002/eqe.2222
Voyagaki E, Vamvatsikos D. Probabilistic assessment of rocking response for simply-supported rigid blocks. SECED 2015 Conference: Earthquake Risk and Engineering towards a Resilient World, Cambridge UK, 2015.
Wan X, Astroza R, Huchinson T, Conte J, Bachman R. Seismic demands on acceleration-sensitive nonstructural components using recorded building response data – Case study. 10th U.S. National Conference on Earthquake Engineering, Anchorage, Alaska, 2014.
Yim C-S, Chopra AK, Penzien J. Rocking response of rigid blocks to earthquakes. *Earthquake Engineering and Structural Dynamics*, 8(6): 563–587, 1980. https://doi.org/10.1002/eqe.4290080606

STATEMENTS AND DECLARATIONS

Funding

This research has been co-financed by the European Regional Development Fund of the European Union and Greek national funds through the Operational Program Competitiveness, Entrepreneurship and Innovation, under the call RESEARCH – CREATE – INNOVATE (project code: T1EDK-00956), project: "ARCHYTAS: Archetypal telemetry and decision support system for the protection of monumental structures". Financial support has been also provided by the European Framework Programme for Research and Innovation (Horizon 2020) project "HYPERION–Development of a decision support system for improved resilience & sustainable reconstruction of historic areas to cope with climate change & extreme events based on novel sensors and modelling tools", Grant Agreement number 821054.

Competing Interests

The authors have no relevant financial or non-financial interests to disclose

Author Contributions

All authors contributed to the study conception and design. The analyses of the rocking blocks were performed by Christos G. Lachanas. The analytical expressions were derived by Athanasia K. Kazantzi. The first draft of the manuscript was written by Athanasia K. Kazantzi and all authors commented on previous versions of the manuscript. All authors read and approved the final manuscript.

Data availability

The datasets generated and analysed during the current study are available from the corresponding author on reasonable request.